JOURNAL OF BACTERIOLOGY, Feb. 2006, p. 1607–1614 Vol. 188, No. 4
0021-9193/06/$08.00+0 doi:10.1128/JB.188.4.1607–1614.2006

The Crystal Structure of the Zinc Phosphodiesterase from *Escherichia coli* Provides Insight into Function and Cooperativity of tRNase Z-Family Proteins

Brenda Kostelecky,[1]† Ehmke Pohl,[2] Andreas Vogel,[1]‡ Oliver Schilling,[1]§ and Wolfram Meyer-Klaucke[1]*

EMBL Hamburg Outstation, c/o DESY, Notkestrasse 85, D-22603 Hamburg, Germany,[1] *and Paul Scherrer Institut, CH-5232 Villigen PSI, Switzerland*[2]

Received 3 August 2005/Accepted 28 November 2005

The *elaC* gene product from *Escherichia coli*, ZiPD, is a 3′ tRNA-processing endonuclease belonging to the tRNase Z family of enzymes that have been identified in a wide variety of organisms. In contrast to the *elaC* homologue from *Bacillus subtilis*, *E. coli elaC* is not essential for viability, and although both enzymes process only precursor tRNA (pre-tRNA) lacking a CCA triplet at the 3′ end in vitro, the physiological role of ZiPD remains enigmatic because all pre-tRNA species in *E. coli* are transcribed with the CCA triplet. We present the first crystal structure of ZiPD determined by multiple anomalous diffraction at a resolution of 2.9 Å. This structure shares many features with the tRNase Z enzymes from *B. subtilis* and *Thermotoga maritima*, but there are distinct differences in metal binding and overall domain organization. Unlike the previously described homologous structures, ZiPD dimers display crystallographic symmetry and fully loaded metal sites. The ZiPD exosite is similar to that of the *B. subtilis* enzyme structurally, but its position with respect to the protein core differs substantially, illustrating its ability to act as a clamp in binding tRNA. Furthermore, the ZiPD crystal structure presented here provides insight into the enzyme's cooperativity and assists the ongoing attempt to elucidate the physiological function of this protein.

The precise cleavage of precursor tRNA (pre-tRNA) after its transcription at both the 5′ and 3′ extensions by specific nucleases is a vital step in the maturation of tRNA (18). tRNase Z, a member of the metallo-β-lactamase superfamily, has been identified as an important endonuclease which cleaves the 3′ extension from various tRNA precursors (24). tRNase Z enzymes have been functionally characterized from a number of both bacterial and archaeal organisms, as well as eukaryotes, including humans (31).

In most cases, tRNase Z proteins cleave the 3′ extension solely from pre-tRNA molecules that lack the CCA triplet. This CCA triplet is the sequence that is present at the 3′ end of all mature tRNA molecules (30), and it is vital for association of tRNA with the large ribosomal subunit during translation (10, 19). While some tRNAs undergo 3′ cleavage followed by addition of the CCA triplet, some archaeal and bacterial tRNAs contain an encoded CCA triplet, and the majority of these tRNAs require neither cleavage by tRNase Z nor subsequent CCA addition. With the exception of *Thermotoga maritima*, all tRNase Z enzymes characterized in this respect to date cleave only pre-tRNA lacking the CCA triplet in vivo (17, 25).

The *Escherichia coli elaC* gene product, designated ZiPD (34), ecoZ (24), tRNase Z (17), or RNase BN (9), is unique in this respect because although all *E. coli* tRNAs are transcribed with an encoded CCA triplet, recombinant *E. coli* ZiPD has been shown to be capable of binding and cleaving only exogenous pre-tRNA which does not contain a CCA triplet (17, 27, 31). Although limited tRNase Z activity has been found in vivo (13, 16), after deletion of the *elaC* gene in *E. coli* neither changes in growth characteristics nor changes in the transcriptome or proteome of the organism have been detected (26). This is in contrast to what occurs in *Bacillus subtilis*, in which deletion of the homologue of the *elaC* gene, *ygjK*, resulted in a nonviable phenotype (21). In this organism, one-third of the tRNA genes do not contain the CCA triplet and thus require tRNase Z cleavage as a maturation step. These findings highlight the interest in detailed characterization of the exceptional *E. coli* ZiPD protein in order to understand the functional and structural relationships within the tRNase Z-protein family.

ElaC from *E. coli* was designated ZiPD based on its zinc-dependent phosphodiesterase activity (34). Although the physiological function of *E. coli* ZiPD remains unknown, the activity and biochemical properties of the protein have been well studied. ZiPD was found to be an effective phosphodiesterase due to its ability to cleave the chromogenic substrates bis(*p*-nitrophenyl)phosphate (bpNPP) and thymidine-5′-*p*-nitrophenylphosphate (34). Kinetic data from the same study showed that there was allosteric activity of the dimeric unit toward bpNPP, and a subsequent study showed that mutation of the His248 and His270 residues to alanine residues eliminated the enzyme's cooperativity (33).

It has recently been shown that the enzyme designated RNase BN is transcribed from the *elaC* gene in *E. coli*; thus, ZiPD and RNase BN are the same enzyme (9), a finding which significantly increases the pool of information available for ZiPD. Despite evidence demonstrating that RNase BN is capable of acting as a backup to the four additional 3′ tRNA

* Corresponding author. Mailing address: EMBL Hamburg Outstation c/o DESY, Notkestrasse 85, D-22603 Hamburg, Germany. Phone: 49 40 8990 2124. Fax: 49 40 8990 2149. E-mail: wolfram@embl-hamburg.de.

† Present address: Cancer Research UK, 44 Lincoln's Inn Fields, London WC2A 3PX, United Kingdom.

‡ Present address: Max-Planck-Institut für Kohlenforschung, Kaiser-Wilhelm-Platz 1, D-45470 Mülheim/Ruhr, Germany.

§ Present address: Department of Oral Biological & Medical Sciences, University of British Columbia, Vancouver, Canada.

TABLE 1. Summary of data collection statistics for multiple anomalous diffraction and native data sets of ZiPD

Parameter	Inflection	Peak	Remote	Native
Beam line	BW7A[a]	BW7A	BW7A	X06SA[b]
Wavelength (Å)	1.282	1.284	1.129	1.000
Resolution (Å)	20 to 3.0	20 to 3.0	20 to 3.0	50 to 2.9
No. of reflections	109,441	49,383	124,515	312,291
No. of unique reflections	17,927	16,989	18,160	20,193
Completeness (%)	99.5 (100)[c]	93.8 (97.7)	99.5 (99.9)	99.8 (99.9)
I/σ (I)	22.7 (2.7)	17.6 (1.5)	27.1 (1.8)	23.4 (3.6)
R_{merge}[d]	0.067 (0.79)	0.057 (0.66)	0.049 (0.88)	0.071 (0.75)

[a] EMBL Hamburg Outstation, DESY.
[b] Swiss Light Source at Paul Scherrer Institut.
[c] The numbers in parentheses correspond to the last resolution shell.
[d] $R_{merge}(I) = \sum_{hkl}\sum_{i} | I_i(hkl) - \overline{I(hkl)} | / \sum_{hkl}\sum_{i} I_i(hkl)$.

maturation enzymes in *E. coli* by cleavage of the 3′ extension from pre-tRNA (13, 16), this activity is inefficient, and the physiological significance of this finding remains unclear. Previous studies on RNase BN also showed that this enzyme is capable of cleaving substrates with the short 3′ elongations tRNA-CU and tRNA-CA with much higher efficiency than it cleaves tRNA-CCA (2), an intriguing finding in light of the fact that all *E. coli* tRNA genes contain the CCA triplet.

The tRNase Z-family proteins belong to the metallo-β-lactamase superfamily, a diverse group of enzymes which catalyze a wide variety of reactions. These enzymes can act in several types of hydrolytic reactions, as well as in redox reactions (1). The defining characteristics of the family are a common metallo-β-lactamase αβ/βα sandwich fold consisting of a set of external α-helices, two internal β-sheets, and a mono- or binuclear metal binding site. Although the primary amino acid sequences of metallo-β-lactamase proteins can be quite diverse, the metal binding motif HXHDH is one of the few highly conserved sequence patterns (1). ZiPD utilizes this metal binding motif to coordinate zinc, a cofactor vital for maximal activity (34). The zinc coordination of ZiPD has been extensively studied, and mutational and spectroscopic studies have shown that the enzyme contains a binuclear zinc site at which one zinc ion is coordinated by three histidine residues and the second zinc ion is coordinated by an aspartate and two additional histidines. Furthermore, the two zinc ions are bridged by a second aspartate with a metal-metal distance of 3.3 Å (33).

ZiPD possesses an exosite, a domain extending from the main body of the protein, which is essential for tRNA recognition but is not required for the intrinsic phosphodiesterase activity or for dimerization (27). This exosite is unique to the tRNase Z proteins in the metallo-β-lactamase family. There are three types of tRNase Z exosites, the ZiPD type, the ElaC2 type, and the TM type, and each type is defined by its length and sequence characteristics. The striking differences between these exosite types are that the ZiPD-type exosite is about 20 amino acids longer than the TM-type exosite and contains a proline-rich region but lacks a basic residue-rich region found in the TM-type exosite, whereas the ElaC2-type exosite is considerably longer than the other two types of exosites but contains the proline-rich region found in the ZiPD-type exosite. A sequence comparison of the exosite regions of tRNase Z-family proteins showed that while the *E. coli* and *B. subtilis* enzymes both contain ZiPD-type exosites, *T. maritima* has a TM-type exosite (27). A sequence analysis in the same study of the human *elaC2* gene, whose protein product is considered a long tRNase Z (tRNase ZL) and is twice the length of a typical "short tRNase Z" (tRNase ZS) with both ends displaying high homology to the tRNase ZSs, revealed a ZiPD-type exosite in the amino-terminal domain and an ElaC2-type exosite in the carboxy-terminal domain.

Very recently, the first crystal structures of tRNase Z were published. The enzymes from *B. subtilis* and *T. maritima* have the typical αβ/βα sandwich fold characteristic of the metallo-β-lactamase family (8, 11). The exosite was resolved in one monomer of *B. subtilis* tRNase Z and was shown to extend from the main body of the dimer opposite the metal binding site. The *T. maritima* crystal structure showed the majority of the protein core, but the model lacks the exosite. Modeling of *B. subtilis* tRNase Z docked with a tRNA molecule suggested a possible binding mode in which the exosite acts as a clamp to lock pre-tRNA into the correct orientation for catalysis, using one monomer to bind the substrate and the other to catalyze hydrolysis with the homodimer capable of cleaving two pre-tRNA molecules at once (8).

In this paper we describe the first crystal structure of *E. coli* ZiPD determined at a resolution of 2.9 Å by multiple anomalous diffraction and refined to an R factor of 23.0%. The structure shares the same overall fold with the homologous enzymes from *B. subtilis* and *T. maritima*, but there are distinct differences. The structure of ZiPD presented here allowed the first detailed comparison of tRNase Z-family structures and provided novel insight into how structural features are related to function in the tRNase Z-protein family.

MATERIALS AND METHODS

Materials. Except where indicated otherwise, all enzymes and fine chemicals were purchased from Sigma. Restriction enzymes were obtained from New England Biolabs (Frankfurt, Germany). Oligonucleotides were synthesized by Genset (Paris, France). DNA sequencing was performed by MWG (Ebersberg, Germany).

Protein purification and crystallization. Expression in *E. coli* was performed as described previously (34). For crystallization experiments protein purification was optimized as follows: 70 μM zinc acetate was added to the buffers for lysis and affinity chromatography, and 10 μM zinc acetate and 10% glycerol were added to the gel filtration buffer to stabilize the protein solution. After gel filtration the protein concentration was adjusted to 25 mg/ml, as determined by the Bradford assay (3), using an ultrafiltration device (Vivascience). Initial microcrystals were obtained from condition 16 from an Emerald Cryo II screen (Emerald Biosystems, Washington) at 4°C and were optimized after that using solutions prepared in the laboratory. The crystals used for data collection were obtained using the hanging-drop vapor diffusion method by mixing 2 μl of an

TABLE 2. Summary of refinement statistics for the native ZiPD data at a resolution of 2.9 Å

Parameter	Value
Unit cell	$a = 147.2$, $b = 147.2$, $c = 138.2$
Space group	$P6_422$
No. of protein residues	305
No. of protein atoms	2,268
Resolution range (Å)	50 to 2.9
No. of observations (total)	20,037
No. of observations for R_{work}	19,099
No. of observations for R_{free}	974
R_{work}	0.23
R_{free}	0.25
RMSD for bond lengths (Å)	0.01
RMSD for bond angles (Å)	1.6

8-mg/ml protein solution in gel filtration buffer and 2 μl of reservoir solution (0.8 M ammonium sulfate, 9% [vol/vol] polyethylene glycol 400, 10% [vol/vol] glycerol, 100 mM imidazole [pH 8.5], 0.5 mM zinc acetate). Full-size crystals that were approximately 150 μm by 40 μm by 40 μm were obtained after 3 weeks of incubation at 4°C. Crystals were soaked for 1 min in the cryobuffer (1.0 M ammonium sulfate, 100 mM imidazole [pH 8.5], 9% [vol/vol] polyethylene glycol 400, 20% [vol/vol] ethylene glycol) and then mounted in nylon loops (32) and immediately cooled in liquid nitrogen.

Data collection. A three-wavelength MAD data set at the Zn edge was collected to an effective resolution of 3.2 Å at EMBL wiggler beamline BW7A (22). Higher-resolution native data at a Bragg spacing of 2.9 Å were collected at SLS beamline X06SA. As the crystals suffered from radiation damage, diffraction data were collected in two batches from the same crystal translated by 80 μm along the long crystal dimension. The MAD data were processed using DENZO and Scalepack (20), and the higher-resolution native data were processed with XDS (12a). F_As were calculated using XPREP, and the substructure was subsequently solved with SHELXD (28). After solvent flattening and phase extension with SHELXE (29), an interpretable density map was obtained. Subsequent iterative cycles of model building using O (12) and crystallographic refinement with CNS (6) resulted in a final model that yielded an R factor of 23% and an R_{free} value of 25%, respectively (4, 5). Further details of the crystal structure determination are summarized in Tables 1 and 2. Figures were prepared using PyMOL (7).

Protein structure accession number. Coordinates have been deposited at the Protein Data Bank (code, 2 cbn).

RESULTS

Quality of the model. The final model is comprised of the complete trace from residue 1 to residue 305 in addition to two residues belonging to the N-terminal tag. The functional dimer is generated by a crystallographic twofold axis, and each active site contains two fully occupied zinc coordination sites. Although the exosite domain showed weaker density, the entire chain could be traced; however, it displayed significantly higher B-factors in this area. Due to the limited resolution (2.9 Å), a number of polar side chains did not show electron density, and thus these residues were refined as alanines. The model possesses good geometry as evaluated by Procheck (15) with all but two residues in the allowed regions of the Ramachandran plot (23). Further details of the structure solution and refinement are summarized in Tables 1 and 2.

Overall crystal structure of ZiPD. ZiPD is a homodimer in which each monomer exhibits the typical metallo-β-lactamase fold, with a core of two seven-strand β-sheets flanked on each side by α-helices (Fig. 1A). The two sheets have similar topologies, consisting of four antiparallel β-strands followed by three parallel β-strands. The exosite extends from the body of the protein between β-strands β9 and β12. The protein core width is approximately 50 Å, and its height and depth are about 32 Å and 28 Å, respectively; the exosite extends from the core of the protein at a slight angle and has a total length of approximately 40 Å. The ZiPD dimerization interface is in the region of helices α1, α2, and α3, and the dimer is arranged with the monomers in a head-to-head fashion with the exosite tails extending away from each other. A narrow cleft is formed jointly by the two monomers in which the active site and metal coordination residues are present (Fig. 1B). In addition, another narrow cleft corresponding to the proposed 3′ trailer RNA binding channel of the *B. subtilis* tRNase Z enzyme (8) is located directly adjacent to this active site cleft and is formed by a single monomer using the loop between α3 and β6 and several residues from the α2 helix.

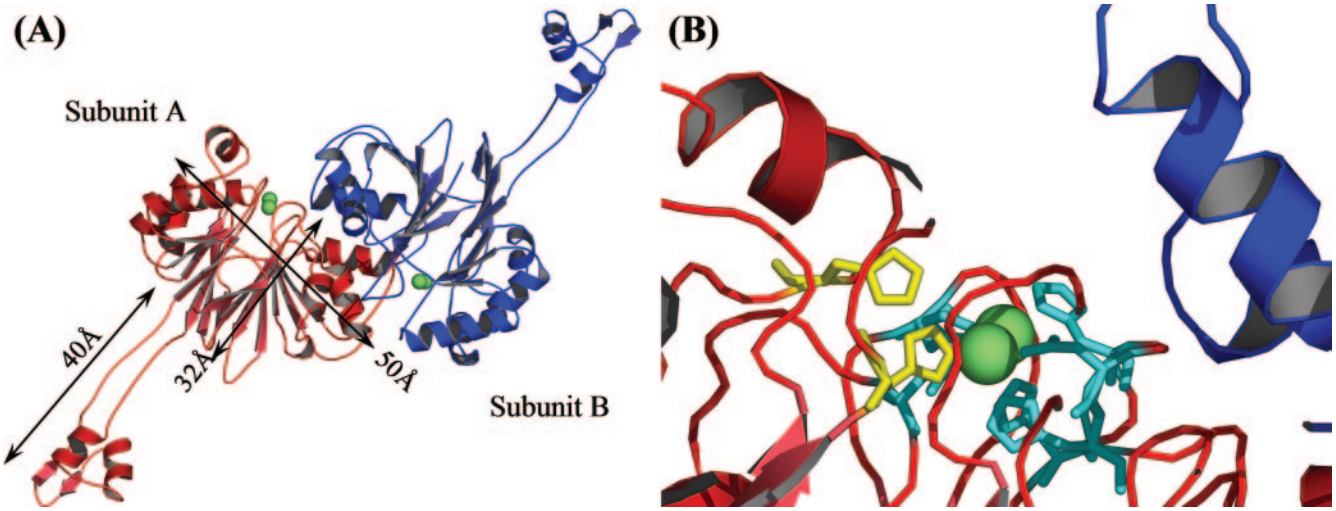

FIG. 1. (A) Ribbon diagram of the crystal structure of the ZiPD homodimer at a resolution of 2.9 Å. Subunit A is red, subunit B is blue, and the zinc ions are represented by green spheres. (B) Active site cleft 1 of ZiPD homodimer formed jointly by subunits A and B. His248 and His 270, which are essential for cooperativity, are yellow, and the remaining zinc ligands are represented by cyan sticks.

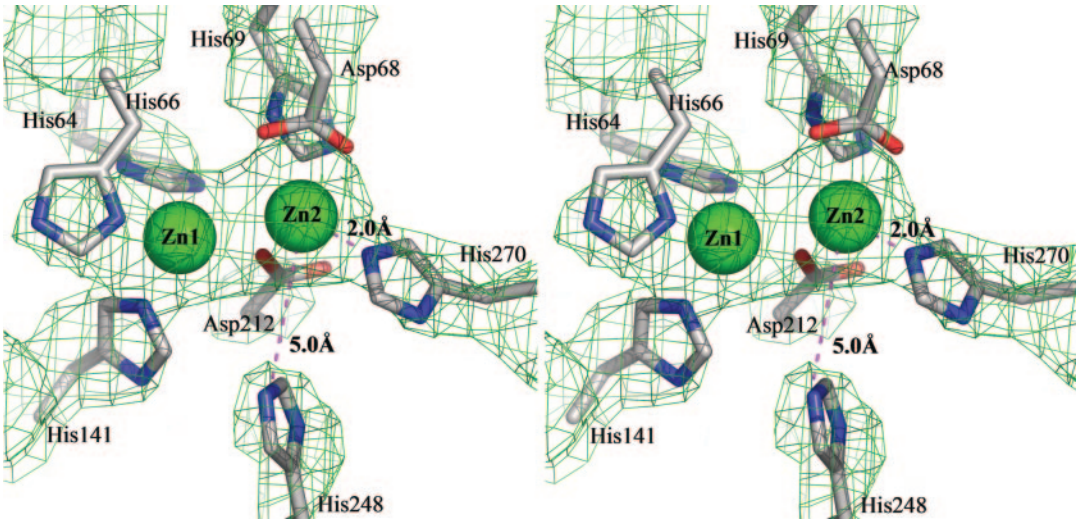

FIG. 2. Stereo view of ZiPD zinc coordination site with the experimental electron density map shown at 1σ above the mean. Zinc ions are represented by green spheres. Bond lengths (in angstroms) between Zn2 and His270 and between Zn2 and His248 are indicated to update previous spectroscopic and mutational analyses in which determining which of the two residues coordinates zinc was impossible.

Each monomer is bound to two zinc atoms located in the groove between the two β-sheets on the side of the monomer facing away from its extended exosite (Fig. 1). Zn1 is coordinated by three histidines (His64, His66, and His141), Zn2 is coordinated by two histidines (His69 and His270) and an aspartate (Asp68), and an additional aspartate (Asp212) bridges the two zinc ions (Fig. 2), which confirms previous spectroscopic and mutational analyses of the metal site (33).

Comparison of known tRNase Z-protein structures reveals that ZiPD shares key tRNase Z features. At the level of protein sequence, *E. coli* ZiPD is 48% and 24% identical to tRNase Z from *B. subtilis* and *T. maritima*, respectively, indicating that there is clear homology (Fig. 3). A comparison of the three-dimensional structures of the three enzymes revealed many surprising similarities and various significant differences. Not only do the three proteins share the metallo-β-lactamase fold, but the numbers of α-helices and β-sheets are equal, the geometry is similar, and each protein contains an exosite which extends from the protein core between β9 and β12 (Fig. 4). All three proteins are homodimers, and the parts are arranged in the same head-to-head fashion, with the exosites of the *E. coli* and *B. subtilis* enzymes extending away from the protein core. The root mean square deviation (RMSD) values between the ZiPD protein core and the cores of the *B. subtilis* and *T. maritima* enzymes (excluding exosite residues 154 to 204 [ZiPD num-

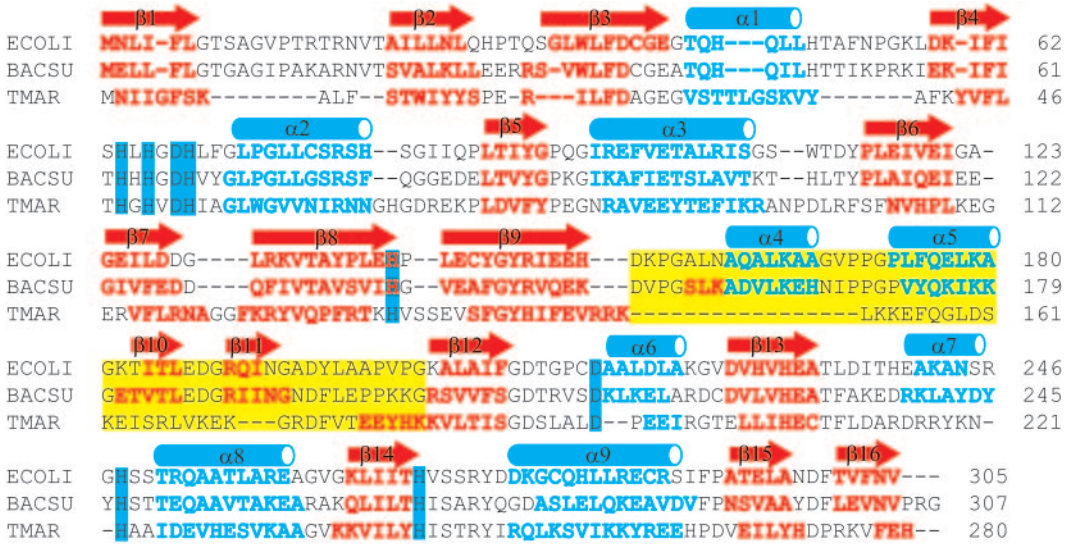

FIG. 3. Sequence alignment of tRNase Z-family proteins. ECOLI, *E. coli* ZiPD; BACSU, *B. subtilis* tRNase Z; TMAR, *T. maritima* tRNase Z. Conserved metal coordinating residues are highlighted in blue, and exosite residues are indicated by a yellow background. Secondary structure features are indicated by red arrows for β-strands and by blue cylinders for α-helices. unknown.

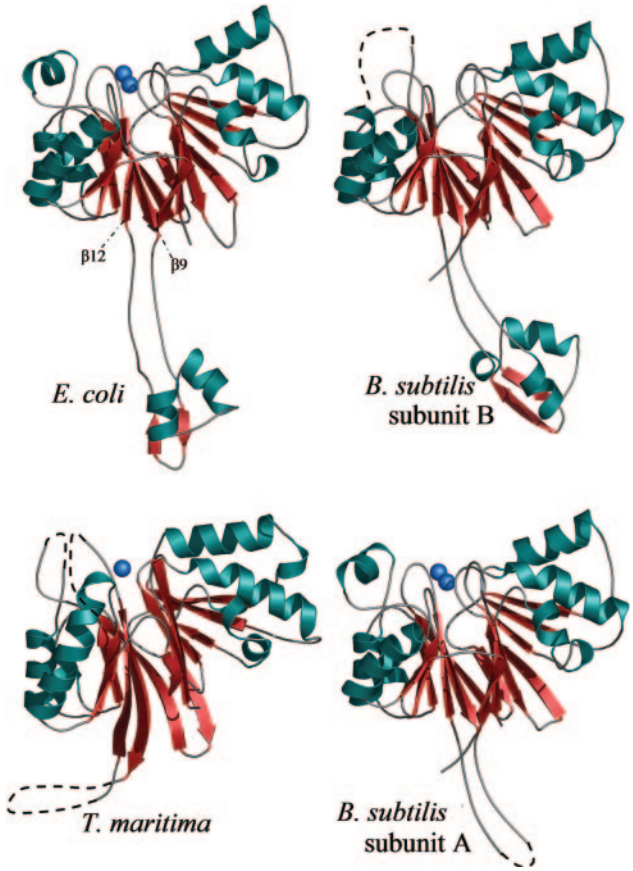

FIG. 4. Comparison of the structures of tRNase Z-family proteins *E. coli* ZiPD, *B. subtilis* tRNase Z (subunits A and B) (8), and *T. maritima* tRNase Z (11). The RMSD values for the protein cores were calculated to be 1.0 Å for *E. coli-B. subtilis* (subunit B) using 254 carbon alpha atoms and 2.1 Å for *E. coli-T. maritima* using 241 carbon alpha atoms. The location of the exosite with respect to the protein core is indicated in the *E. coli* ZiPD diagram by dotted lines.

bering]) are 1.0 Å and 2.1 Å, respectively, as calculated by the protein structure comparison service SSM at the European Bioinformatics Institute (14). The RMSD value between the exosites from ZiPD and *B. subtilis* tRNase Z is 1.5 Å. The lengths and structures of the ZiPD and *B. subtilis* exosites are similar, and the most remarkable difference is the 20° difference in the angle between the exosites and the corresponding protein cores (Fig. 5). This difference highlights the intrinsic flexibility of the exosite, a feature likely to be necessary for substrate recognition and binding.

A feature observed solely in *B. subtilis* tRNase Z and not seen in ZiPD is a conformational difference between the two monomers, which includes a distortion of one metal binding site. His140 (homologous to His141 in *E. coli*) is displaced by about 8 Å, which prevents the binding of zinc and renders the subunit inactive. This conformation is present in both domains of *T. maritima* tRNase Z and is also presumably inactive, given the conservation of metal coordinating residues. The monomers of ZiPD, in contrast, display crystallographic symmetry and contain intact and fully occupied metal sites.

FIG. 5. Superposition of ZiPD and *B. subtilis* tRNase Z carbon alpha chains. ZiPD is blue, and tRNase Z is yellow. The RMSD value between the exosites was calculated to be 1.5 Å using the carbon alpha atoms of 51 residues.

DISCUSSION

ZiPD crystal structure highlights the key role that the exosite plays in the function of tRNase Z-family enzymes. The most intriguing feature of the ZiPD crystal structure is the flexible exosite, which extends from each monomer's core and is essential for tRNA recognition (27). A comparison with the structure and sequence of *B. subtilis* tRNase Z showed that the lengths of the two exosites are equivalent and that in both exosites there is a region rich in proline residues located between the α-helices. The fact that the conserved proline-rich region is between the two exosite helices indicates that the helices must be at a rigid angle relative to each other, a feature which is likely vital to the exosite's ability to bind its substrate.

Superposition of the two structures shows the exosites at different angles with respect to the main body of the protein (Fig. 5). The difference in angles with respect to the core domain of the two static structures, along with evidence of high B-factors within the exosite neck and the poorly defined electron density in the exosite region of the various tRNase Z structures solved so far, highlights the likelihood that the exosite neck is flexible and indicates that it moves freely between conformations in solution. In the case of the ZiPD structure, this free movement was likely stabilized by crystal contacts between the exosites of neighboring dimers, allowing resolution of this domain. Based on this evidence of the exosite's flexibility and previous studies showing its vital role in tRNA binding and recognition, we support the model in which the exosite's flexibility in solution allows it to act as a clamp which

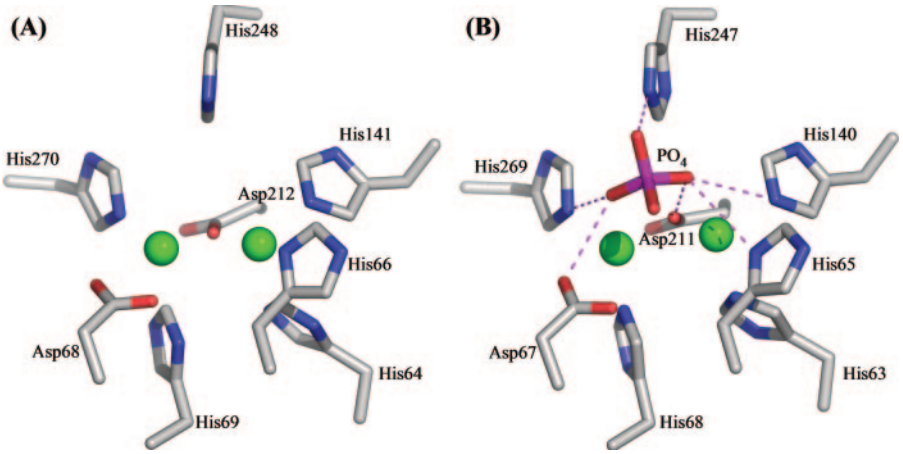

FIG. 6. Comparison of active sites with and without PO_4 bound from *E. coli* ZiPD (A) and *B. subtilis* tRNase Z subunit B (bound to PO_4) (B). Hydrogen bonds to the phosphate molecule are magenta and highlight the key role of His248 and His270 in determining substrate orientation.

utilizes the rigid conformation of α-helices and β-strands at its end to effectively recognize and bind its substrate and the flexible exosite neck to guide the substrate into an orientation optimal for catalysis.

As a result of these and other recent findings with regard to the ZiPD exosite, an examination of the exosite's role in the larger context of the tRNase Z-family enzymes is of considerable interest. The fact that this structure shows that ZiPD is a dimer in which the exposed part of the active site cleft faces the exosite of the adjacent monomer (Fig. 1) supports the model proposed in the *B. subtilis* tRNase Z structural study (8), in which the pre-tRNA is bound by the exosite of one monomer and processed by the active site of the second monomer, which allows two pre-tRNA molecules to be processed at once. Also interesting with regard to the tRNase Z-family exosites is the fact that all enzymes characterized so far containing the ZiPD-type exosites process tRNA lacking the CCA triplet, whereas the *T. maritima* enzyme, for which the TM-type exosite was named, processes tRNA molecules containing a CCA triplet, a difference possibly related to the fact that the exosite types have different lengths and conserved motifs. At this point, how the exosite plays a role in substrate specificity is a matter of pure speculation given that all models to date point away from the hypothesis that the exosite interacts directly with the 3′ end of the pre-tRNA molecule. The role of the exosites in the tRNase ZL enzymes is even less obvious given the fact that two different types of exosites are present. Speculation on how these exosite types determine substrate orientation and whether they assist in determining specificity is therefore beyond the scope of this study, but these questions are certainly important in future research on the tRNase Z family.

His248 and His270 may contribute to ZiPD cooperativity by dictating substrate orientation. Both His248 and His270 have been implicated in the cooperativity of ZiPD with the substrate bpNPP. Alanine mutations of each of these residues eliminated cooperativity, while alanine mutations of all other metal ligands resulted in Hill coefficients comparable to that of wild-type ZiPD (33). This finding indicates that the binding of bpNPP and possibly other substrates to His248 and His270 causes a conformational change in the dimer which increases the affinity of the second active site for its substrate. The *B. subtilis* tRNase Z structure, in which one subunit is crystallized with a phosphate ion bound in the active site, shows that His247 and His269 (corresponding to His248 and His270 in the *E. coli* enzyme) form hydrogen bonds with the phosphate molecule (8) (Fig. 6), a conformation which the phosphate group of a pre-tRNA substrate molecule would also likely adopt. This rearrangement of hydrogen bonds in subunit A upon phosphate binding does not, however, appear to change its conformation significantly enough to affect the region of subunit A involved in forming the second active site cleft. In addition, His248 and His270 lie on the edge of the active site residues farthest from the dimerization interface (Fig. 1B), ruling out the possibility that their movement directly affects the conformation of subunit B.

Given this information, it is possible that His248 and His270 assist in cooperativity by positioning the substrate in such a way that steric hindrance within the interface formed by the two monomers forces a slight shift in the orientation of the second subunit with respect to the first subunit in order to accommodate the substrate. This would cause an identical change in the second active site, increasing its affinity for the substrate by relieving the steric hindrance originally present at the dimerization interface near the second active site. In this model, the binding of the first substrate would cause a dimerization shift that allows a second substrate molecule to have easier access to the second active site, and the two pre-tRNA molecules could be processed at once.

ZiPD is the first tRNase Z-family crystal structure with fully intact and occupied metal coordination sites. Interestingly, the structures of *B. subtilis* tRNase Z, in which variation between the two subunits was observed, and ZiPD, whose monomers are identical, are different. Of particular interest is the fact that in the *B. subtilis* tRNase Z structure, the variation between the monomers includes a distortion of the active site of one monomer so that it is incapable of binding zinc. This difference is not likely due to crystal packing since neither structure contains crystal contacts in the region of variance.

Previously, it was postulated that substrate binding to the first active site would cause a conformational change which

would align the second zinc coordination sphere, allowing two additional zinc molecules and a second substrate molecule to bind, explaining the allosteric behavior of the protein (8). The fact that the present structure of ZiPD clearly shows the second zinc coordination sphere intact and fully loaded with zinc in the absence of substrate indicates that restoration of the *B. subtilis* tRNase Z metal binding site is not likely accomplished by conformational changes brought on by substrate binding; rather, it is more likely that the distortion of the active site in *B. subtilis* tRNase Z represents an inactive form of the enzyme or an intermediate whose role is not known yet. Consequently, ZiPD represents the first crystal structure of a member of the tRNase Z family with intact and fully occupied metal binding sites, a state which likely represents the fully active enzyme.

Implication of the ZiPD structure in the search for the physiological role of ZiPD. ZiPD has high structural similarity to tRNase Z of *B. subtilis*, yet both in vitro evidence and in vivo evidence demonstrated that ZiPD does not play the same essential role in maturation of the 3′ end of tRNA even though ZiPD is expressed in *E. coli* at basal levels. Based on its strong structural similarity to tRNase Z enzymes and its ability to bind tRNA and to process CCA-less tRNA in vitro, the physiological function of ZiPD is almost certainly related to the processing of tRNA.

It was proposed, based on the docking model of *B. subtilis* tRNase Z with tRNA, that the loop between β1 and β2 could be responsible for the inhibition of CCA-containing pre-tRNAs (8). In the *T. maritima* enzyme there is in fact a shorter secondary structure element in this region which would allow the cleft to accommodate CCA-containing pre-tRNAs. ZiPD exhibits a loop in this region that is very similar to that of the *B. subtilis* enzyme, supporting the view that CCA is also an antideterminant for the *E. coli* enzyme and reaffirming the assumption that ZiPD does not play the same role in tRNA processing since all tRNA genes in *E. coli* encode the CCA triplet.

In light of what is known about ZiPD's ability to cleave pre-tRNA species which contain incorrect nucleotides in place of the CCA sequence, it is very likely that the physiological function of ZiPD is to perform the 3′ cleavage reaction when gene mutation or erroneous transcription causes a mutation in the CCA triplet, a particularly useful trait in conditions that promote an accelerated mutation rate or high tRNA turnover. Thus, the function of ZiPD could be tRNA repair as opposed to maturation, which is typical of tRNase Z enzymes.

However, since proteins in the metallo-β-lactamase family are capable of carrying out a wide range of enzymatic reactions using the same basic chemical and structural mechanisms (1), the possibility that similarly diverse functions may exist within the tRNase Z family, including the possibility that ZiPD cleaves other RNA species, cannot be excluded. Further studies, including additional biochemical experiments, as well as cocrystallization of ZiPD complexed with tRNA, may help establish the factors that determine substrate specificity and confirm the physiological function of ZiPD.

ACKNOWLEDGMENTS

We thank Esben Lorentzen for his valuable input and assistance with figures. In addition, we greatly appreciate support from staff at EMBL beamline BW7A and SLS beamline X065A.

REFERENCES

1. **Aravind, L.** 1999. An evolutionary classification of the metallo-beta-lactamase fold proteins. In Silico Biol. **1:**69–91.
2. **Asha, P. K., R. T. Blouin, R. Zaniewski, and M. P. Deutscher.** 1983. Ribonuclease BN: identification and partial characterization of a new tRNA processing enzyme. Proc. Natl. Acad. Sci. USA **80:**3301–3304.
3. **Bradford, M. M.** 1976. A rapid and sensitive method for the quantitation of microgram quantities of protein utilizing the principle of protein-dye binding. Anal. Biochem. **72:**248–254.
4. **Brunger, A. T.** 1993. Assessment of phase accuracy by cross validation—the free R-value—methods and applications. Acta Crystallogr. Sect. D Biol. Crystallogr. **49:**24–36.
5. **Brunger, A. T.** 1992. Free R-value—a novel statistical quantity for assessing the accuracy of crystal structures. Nature **355:**472–475.
6. **Brunger, A. T., P. D. Adams, G. M. Clore, W. L. DeLano, P. Gros, R. W. Grosse-Kunstleve, J. S. Jiang, J. Kuszewski, M. Nilges, N. S. Pannu, R. J. Read, L. M. Rice, T. Simonson, and G. L. Warren.** 1998. Crystallography & NMR system: a new software suite for macromolecular structure determination. Acta Crystallogr. Sect. D Biol. Crystallogr. **54:**905–921.
7. **DeLano, W. L.** 2002, posting date. The PyMOL molecular graphics system. [Online.] http://www.pymol.org.
8. **de la Sierra-Gallay, I. L., O. Pellegrini, and C. Condon.** 2005. Structural basis for substrate binding, cleavage and allostery in the tRNA maturase RNase Z. Nature **433:**657–661.
9. **Ezraty, B., B. Dahlgren, and M. P. Deutscher.** 2005. The RNase Z homologue encoded by *Escherichia coli elaC* gene is RNase BN. J. Biol. Chem. **280:**16542–16545.
10. **Green, R., and H. F. Noller.** 1997. Ribosomes and translation. Annu. Rev. Biochem. **66:**679–716.
11. **Ishii, R., A. Minagawa, H. Takaku, M. Takagi, M. Nashimoto, and S. Yokoyama.** 2005. Crystal structure of the tRNA 3′ processing endoribonuclease tRNase Z from *Thermotoga maritima*. J. Biol. Chem. **280:**14138–14144.
12. **Jones, T. A., J. Y. Zou, S. W. Cowan, and Kjeldgaard.** 1991. Improved methods for building protein models in electron density maps and the location of errors in these models. Acta. Crystallogr. Sect. A **47:**110–119.

12a. **Kabsch, W.** 1993. Automatic processing of rotation diffraction data from crystals of initially unknown symmetry and cell constants. J. Appl. Crystallogr. **26:**795–800.

13. **Kelly, K. O., and M. P. Deutscher.** 1992. The presence of only one of five exoribonucleases is sufficient to support the growth of *Escherichia coli*. J. Bacteriol. **174:**6682–6684.
14. **Krissinel, E., and K. Henrick.** 2004. Secondary-structure matching (SSM), a new tool for fast protein structure alignment in three dimensions. Acta Crystallogr. Sect. D Biol. Crystallogr. **60:**2256–2268.
15. **Laskowski, R. A., D. S. Moss, and J. M. Thornton.** 1993. Main-chain bond lengths and bond angles in protein structures. J. Mol. Biol. **231:**1049–1067.
16. **Li, Z., and M. P. Deutscher.** 1996. Maturation pathways for *E. coli* tRNA precursors: a random multienzyme process *in vivo*. Cell **86:**503–512.
17. **Minagawa, A., H. Takaku, M. Takagi, and M. Nashimoto.** 2004. A novel endonucleolytic mechanism to generate the CCA 3′ termini of tRNA molecules in *Thermotoga maritima*. J. Biol. Chem. **279:**15688–15697.
18. **Morl, M., and A. Marchfelder.** 2001. The final cut. The importance of tRNA 3′-processing. EMBO Rep. **2:**17–20.
19. **Nissen, P., J. Hansen, N. Ban, P. B. Moore, and T. A. Steitz.** 2000. The structural basis of ribosome activity in peptide bond synthesis. Science **289:** 920–930.
20. **Otwinowski, Z., and W. Minor.** 1997. Processing of X-ray diffraction data collected in oscillation mode. Macromol. Crystallogr. Part A **276:**307–326.
21. **Pellegrini, O., J. Nezzar, A. Marchfelder, H. Putzer, and C. Condon.** 2003. Endonucleolytic processing of CCA-less tRNA precursors by RNase Z in *Bacillus subtilis*. EMBO J. **22:**4534–4543.
22. **Pohl, E., A. Gonzalez, C. Hermes, and R. G. van Silfhout.** 2001. Overview of the tunable beamlines for protein crystallography at the EMBL Hamburg Outstation; an analysis of current and future usage and developments. J. Synchrotron Radiat. **8:**1113–1120.
23. **Ramachandran, G. N., and V. Sasisekharan.** 1968. Conformation of polypeptides and proteins. Adv. Protein Chem. **23:**283–438.
24. **Schiffer, S., S. Rosch, and A. Marchfelder.** 2002. Assigning a function to a conserved group of proteins: the tRNA 3′-processing enzymes. EMBO J. **21:**2769–2777.
25. **Schiffer, S., S. Rosch, and A. Marchfelder.** 2003. Recombinant RNase Z does not recognize CCA as part of the tRNA and its cleavage efficiency is influenced by acceptor stem length. Biol. Chem. **384:**333–342.
26. **Schilling, O., S. Ruggeberg, A. Vogel, N. Rittner, S. Weichert, S. Schmidt, S. Doig, T. Franz, V. Benes, S. C. Andrews, M. Baum, and W. Meyer-Klaucke.** 2004. Characterization of an *Escherichia coli elaC* deletion mutant. Biochem. Biophys. Res. Commun. **320:**1365–1373.

27. **Schilling, O., B. Spath, B. Kostelecky, A. Marchfelder, W. Meyer-Klaucke, and A. Vogel.** 2005. Exosite modules guide substrate recognition in the ZiPD/ElaC protein family. J. Biol. Chem. **280:**17857–17862.
28. **Sheldrick, G. M.** 1998. SHELX: applications to macromolecules, p. 401–411. *In* S. Fortier (ed.), Direct methods for solving macromolecular structures. Kluwer Academic Publisher, Dordrecht, The Netherlands.
29. **Sheldrick, G. M.** 2002. Macromolecular phasing with SHELXE. Z. Kristallogr. **217:**644–650.
30. **Sprinzl, M., C. Horn, M. Brown, A. Ioudovitch, and S. Steinberg.** 1998. Compilation of tRNA sequences and sequences of tRNA genes. Nucleic Acids Res. **26:**148–153.
31. **Takaku, H., A. Minagawa, M. Takagi, and M. Nashimoto.** 2004. The N-terminal half-domain of the long form of tRNase Z is required for the RNase 65 activity. Nucleic Acids Res. **32:**4429–4438.
32. **Teng, T. Y.** 1990. Mounting of crystals for macromolecular crystallography in a freestanding thin-film. J. Appl. Crystallogr. **23:**387–391.
33. **Vogel, A., O. Schilling, and W. Meyer-Klaucke.** 2004. Identification of metal binding residues for the binuclear zinc phosphodiesterase reveals identical coordination as glyoxalase II. Biochemistry **43:**10379–10386.
34. **Vogel, A., O. Schilling, M. Niecke, J. Bettmer, and W. Meyer-Klaucke.** 2002. *elaC* encodes a novel binuclear zinc phosphodiesterase. J. Biol. Chem. **277:** 29078–29085.